Gold Deposition by Galvanic Displacement on Semiconductor Surfaces: Effect of Substrate on Adhesion

L. Magagnin,† R. Maboudian, and C. Carraro*

Department of Chemical Engineering, University of California, Berkeley, California 94720-1462

Received: September 5, 2001; In Final Form: October 30, 2001

Thin gold films are grown on Si and Ge substrates by galvanic displacement from fluoride-containing solutions. The physical and chemical properties of the metal−semiconductor interface are characterized by a variety of techniques, including photoelectron spectroscopy, atomic force microscopy, and electron microscopy. Displaced gold films exhibit strong adhesion to germanium substrates but not to silicon. This behavior is explained by the presence of a chemical bond at the Au−Ge interface, which is not observed in the Au−Si system. The implications of these findings for semiconductor metallization by galvanic displacement methods are discussed.

I. Introduction

The reducing behavior of elemental silicon toward noble metal ions in aqueous solutions containing fluoride ions has long been known.[1−9] Although the detailed mechanism by which metal ions are displaced from solution is still far from understood, the process is thought to be described by the following two half-cell reactions:

$$\text{anodic: } Si + 6HF \rightarrow SiF_6^{2-} + 6H^+ + 4e^-$$

$$\text{cathodic: } Me^{n+} + ne^- \rightarrow Me$$

where Me denotes any metal more noble than H (Table 1).

These reactions are of great interest in microelectronics technology, where the wet etching of the native oxide on Si surfaces is effected by a dip in (possibly buffered) HF solutions. Solution contamination by metallic ions can lead to undesirable deposition of noble metal impurities on the Si surface, compromising the performance of electronic devices. Thus, it is not surprising that much recent work has focused on the growth of metallic nanoclusters from very dilute solutions of metal ions.[11−13] Deposition of copper and gold films from fluoride solutions on silicon and germanium was studied by Balashova et al.[14] and Krikshtopaitis et al.[15] about thirty years ago. The kinetics of gold accumulation depended to a large extent on the surface of the specimen. A reduction in the metal precipitation rate with time was observed both for silicon and germanium. The evaluation of the germanium potential during deposition indicated that the reduction of gold ions took place predominantly by charge transfer through the valence zone of the electrode. Recent work has rekindled interest in the possibility of growing relatively thick metallic films on Si by the galvanic displacement process described by the above reactions. This process possesses several desirable features, which make it competitive with state of the art physical or electrochemical deposition processes: it is substrate selective, very conformal, and does not require seed layers.

TABLE 1: Redox Potentials for All Metals More Noble than Hydrogen (referred to the hydrogen standard electrode)[a]

element	redox potential (V vs NHE)
Au	Au^{3+}/Au, 1.42
Pt	Pt^{2+}/Pt, 1.18
Ir	Ir^{4+}/Ir, 0.93
Pd	Pd^{2+}/Pd, 0.83
Ru	Ru^{2+}/Ru, 0.80
Ag	Ag^{+}/Ag, 0.79
Rh	Rh^{3+}/Rh, 0.76
Cu	Cu^{2+}/Cu, 0.34
Ge	Ge^{4+}/Ge, 0.12
Re	Re^{3+}/Re, 0.30
Ni*	Ni^{2+}/Ni, −0.23
Si	SiF_6^{-2}/Si, −1.20

[a] If the redox potential is negative, hydrogen evolution dominates over metal displacement. Nickel can be displaced on silicon in fluoride-containing solutions at pH = 8.[10]

The nature of the silicon-metal interface obtained in the galvanic displacement process remains poorly understood. Our recent work[16] on displaced Cu films on Si indicates that the mechanical properties of the interface, specifically adhesion, are rather poor. However, when particular additives were included in the plating bath, excellent substrate adhesion was achieved. The role of these additives (namely ascorbic acid for Cu deposition) on film−substrate adhesion remains unexplained.

In view of the technological interest in this process,[17] and of the fact that a wide combination of semiconductor/metal interfaces can be achieved based on the redox potentials listed in Table 1, it would be highly desirable to gain a fundamental understanding of the principles that govern the adhesion of the films at the atomic level. This paper is a step in this direction.

Here, we study Au films deposited on Si(111) and on Ge(111) surfaces by the galvanic displacement method. Our main findings are that while the Au/Si interface formed in this process is exceedingly weak, displaced Au films adhere very strongly to the surface of Ge, even in the thick film regime. Using valence band X-ray photoelectron spectroscopy, we are able to determine the formation of a chemical bond between Au and Ge atoms. In contrast, no perturbation of the core or valence band electronic structure is detected at the Si−Au interface. We hypothesize that good adhesion of displaced films on Si (or Ge) can be

* Corresponding author. E-mail: carraro@cchem.berkeley.edu. Fax: (510) 642-4778.

† Permanent address: Dipartimento di Chimica Fisica Applicata, Politecnico di Milano, Via Mancinelli, 7, 20131 Milano, Italy.

10.1021/jp013396p CCC: $22.00
Published on Web 12/19/2001

obtained for metals with propensity to form stoichiometric compounds at room temperature, such as gold on Ge and palladium and platinum on Si.

II. Experimental Section

Reagent grade chemicals and deionized water were used for the preparation of the plating solutions. Fresh solutions obtained by dissolving 0.1−1 mM potassium tetrachloroaurate ($KAuCl_4$) in 5 M hydrofluoric acid (HF) solution were used for each sample. Single crystalline (111) and (100), p- and n-type, silicon and germanium were used as substrates, as well as LPCVD-grown polycrystalline samples. Samples were cleaned by rinsing with acetone and deionized water, dried with nitrogen flux, and treated for 15 min in a UV−ozone cleaner at room temperature. Before deposition, samples were etched in concentrated HF for 10 min, rinsed with deionized water, and dried. After immersion in the plating solution, samples were carefully rinsed with deionized water and dried with nitrogen. Deposition was performed at room temperature without stirring.

Scanning probe experiments were carried out with a Digital Instruments (DI) atomic force microscope (AFM) operating in tapping mode with silicon cantilevers. Roughness values were obtained by the image analysis tools provided with the instrument. X-ray diffraction (XRD) experiments with Bragg−Brentano configuration were performed in a Philips PW 1830 instrument, with a goniometer (Philips PW 3020) and a control unit (Philips PW 3710) (Cu Kα radiation with wavelength 1.5406 Å, scan rate 1 degree per minute). For the scanning electron microscopy (SEM) experiments, a Cambridge Stereoscan 360 with 10^{-5} to 10^{-10} Torr vacuum was used. Sample cross sections were imaged after fracture in liquid nitrogen.

The X-ray photoelectron spectroscopy (XPS) experiments were performed in an ultrahigh vacuum chamber with base pressure of 10^{-9} Torr, equipped with an Omicron EA125 electron energy analyzer and an Omicron DAR400 source of Al Kα X-rays at an energy of 1486.6 eV. The detector angle was 0° to the surface normal (80° for grazing angle analyses). The spectra were analyzed using curve-fitting with Gaussians to determine peak positions. Deconvolution was performed after subtraction of the background with the Shirley method. The component peak parameters were constrained to experimental values deduced from measurements on reference samples.

A sputtered gold film (1.8 μm thick) was used to calibrate the photoelectron energy. The Au 4f spectrum of sputtered gold was fitted with two Gaussian peaks with doublet separation of 3.7 eV. The fitting curve showed two peaks at 83.9 and 87.6 eV, respectively, for Au $4f_{7/2}$ and Au $4f_{5/2}$, with full width half-maximum (fwhm) of 1.8 eV for both peaks. The C 1s spectrum of sputtered gold was then fitted with three Gaussian peaks at 284.2, 285, and 286.4 eV, with fwhm of 1.8 eV. The peaks at 284.2 and 285 eV correspond to aliphatic carbon. The peak at 286.4 eV is indicative of carbon bonded to oxygen. The peak binding energies and the fwhm of the carbon peak obtained on sputtered gold were used as reference values for the C 1s spectrum of coated or uncoated silicon and germanium samples. In other words, spectra were shifted according to the difference in binding energy between each sample's C 1s peaks and sputtered gold C 1s reference peaks.

III. Results and Discussion

Adhesion of Gold Films. Thin gold films were galvanically deposited for 1 to 30 min on Si(111) and Ge(111) in 1 mM $KAuCl_4$ and 5 M HF solution. Homogeneous and bright yellow deposits were obtained on both silicon and germanium. The adhesion of the gold films was qualitatively evaluated through the scotch tape test with commercial 3M scotch tapes and industrial tapes immediately after the deposition. Some samples were tested again several days following the deposition. A sample failed the tape test if the metallic film was completely peeled off by the tape, exposing the substrate.

Adhesion of the gold films is strictly dependent on the semiconductor type. A sharp distinction between gold on silicon and gold on germanium is observed. Independent of the thickness and plating time, gold films on silicon always failed the tape test, while gold films on germanium always adhered to the substrate and passed the test. Tests were repeated on (100) and polycrystalline p- and n-type substrates, always confirming the behavior of the films on (111) substrates. Hence, adhesion cannot be related to the orientation, doping, or roughness of the semiconductor substrate.

Growth and Structure of Gold Films. The initial nucleation and growth of gold films on Si(111) and Ge(111) were characterized by atomic force microscopy. Samples were imaged after immersion in 0.1 mM $KAuCl_4$ and 5 M HF plating solution (due to the very fast nature of the displacement reaction, the concentration of gold was reduced in order to resolve the initial nucleation stage from the growth stage). Figure 1a,b shows noncontact AFM images of the uncoated silicon and germanium samples respectively after etching in HF. A very flat surface with root-mean-square (rms) roughness of 0.08 nm characterizes the silicon sample, while the rms roughness for germanium is 0.24 nm. Figure 1c,d shows images taken (in air) following deposition for 5 s on silicon and germanium, respectively. The formation of small clusters in the range of 10−30 nm, distributed uniformly across the surface, is observed for silicon substrates. Clusters forming on germanium substrates are more sparsely distributed, though cluster size is still in the range of 10−30 nm. The cluster density on the surface increases with time for both silicon and germanium, as one can observe in Figure 1e,f after deposition for 60 s. The formation of gold films on silicon can be described in terms of clusters nominally distributed all over the active surface. A three-dimensional growth follows the completion of a first cluster layer at the Si surface with overlayers of isolated large structures shown in Figure 1g after 10-minute deposition. Figure 1h shows the germanium surface after 10 min of deposition with formation of overlayers following the island growth mode of the first layer. The rms roughness greatly grows for gold on silicon, from a range of 2 nm after 60 s to about 18 nm after 10 min of plating. The growth of gold on germanium is characterized by rms roughness in the range of 2 nm, even after 10 min of plating.

The effect of the substrate on the structure of thick gold films is evaluated by X-ray diffraction on samples obtained after deposition for 30 min in 1 mM $KAuCl_4$ and 5 M HF plating solution. The XRD patterns on Si(111) and Ge(111) in Figure 2 show a preferential orientation of gold for the (111) plane, the closed packed plane for the face centered cubic structure. Gold on Si(100) shows a preferential orientation for the (100) plane, related to the influence of the substrate. On Ge(100), such preferential orientation is less pronounced, with the presence of a strong (111) plane peak for gold. The full width in radians $B(2\theta)$ subtended by the half-maximum intensity width of the main powder diffraction line is related to the average crystallite size L according to the Scherrer equation:

$$B(2\theta) = K\lambda/(L\cos\theta)$$

where K is the shape factor and usually has a value of 0.94, λ is the X-ray wavelength (1.54 Å), and θ is the Bragg angle.

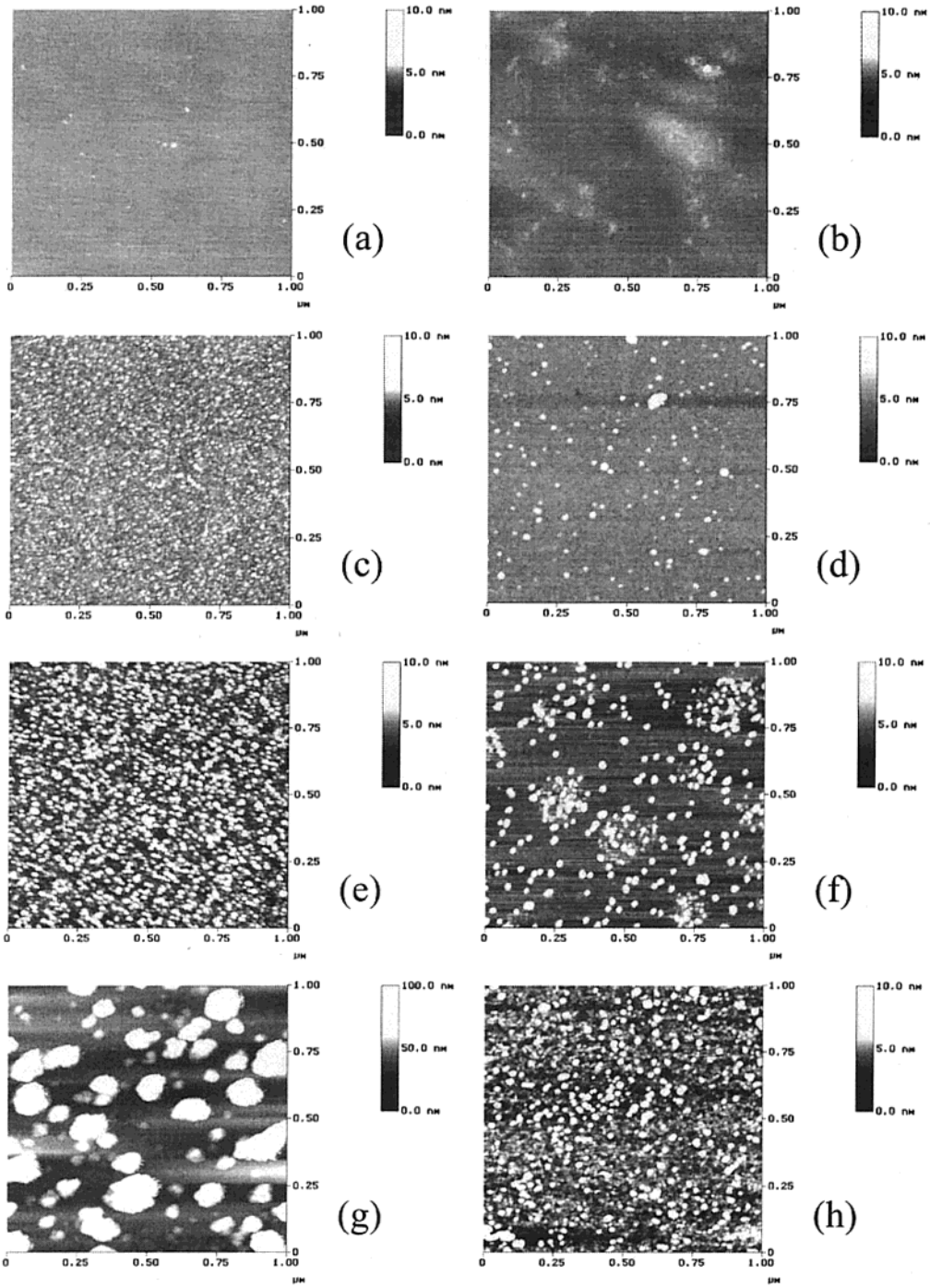

Figure 1. Atomic force micrographs of semiconductor surfaces for various duration of immersion in 0.1 mM Au bath: (a) clean Si(111), rms roughness 0.08 nm; (b) clean Ge(111), rms roughness 0.24 nm; (c) 5 s Si(111), rms roughness 0.84 nm; (d) 5 s Ge(111), rms roughness 0.96 nm; (e) 60 s Si(111), rms roughness 1.7 nm; (f) 60 s Ge(111), rms roughness 1.8 nm; (g) 600 s Si(111), rms roughness 18.9 nm; (600) s Ge(111), rms roughness 1.9 nm.

From the data, an average crystallite size of about 30 nm for Si(111), Si(100), and Ge(111) is estimated. A lower value of about 20 nm characterizes the crystallite size for Ge(100). These values represented an average of various sizes and are in good agreement with the AFM observation of the initial stages of growth.

The SEM images in Figure 3 show the cross sections after fracture of the same samples. The gold films on Si(111) and Ge(100) and (111) are compact and homogeneous with an estimated thickness of about 50 nm. The surface morphology revealed the 3D growth, although the films appeared optically smooth and reflective. A pronounced dendritic growth characterizes gold on Si(100), although the film remained optically similar to the previous ones. The particular structure of the gold film, likely due to the 3D growth, has a strong influence on the electrical resistivity of the films as deposited. Compared to sputtered gold, which exhibits resistivity of about 2.3 $\mu\Omega$ cm (i.e., that of the bulk metal), the displaced gold as deposited is characterized by resistivity values about four times higher.

Photoelectron Spectroscopy: Gold on Silicon and Germanium. The photoelectron spectra were collected on silicon and germanium surfaces immediately after cleaning and etching, and then on the same surfaces after immersion in 0.1 mM $KAuCl_4$ and 5 M HF plating solution. Figure 4 shows the Si 2p

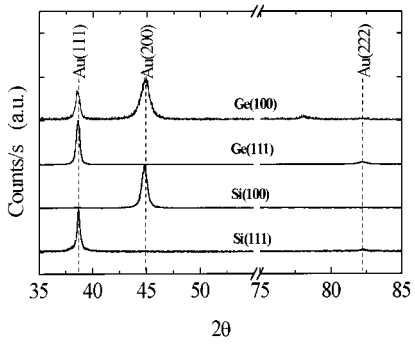

Figure 2. X-ray diffraction 2θ scan for samples after 30 min plating in 1 mM Au bath.

core peak for clean silicon and after 5 and 60 s of immersion into the gold solution. The silicon core level (2p) has a binding energy of 99 eV and remains unshifted with plating. A new peak at 103 eV is observed with increasing amount of gold and is attributed to the formation of silicon dioxide at the surface.

Figure 5 shows the Ge 3d peak for clean germanium and after 5, 60, and 600 s of immersion in the gold solution. The core peak for clean germanium has a binding energy of 29.3 eV. With increasing gold coverage on the surface, the experimental peak is shifted toward higher binding energies. The core peak line shape for gold-covered germanium is then deconvoluted into two Gaussian curves assigned to elemental germanium and to germanium oxide at lower and higher binding energies, respectively. The fitted elemental germanium peak is shifted by 0.2−0.3 eV toward higher binding energies with respect to the clean substrate peak. The formation of germanium oxide is presumed by the small fitted peak at about 31.4 eV, which can be attributed to GeO.

The Au 4f spectra for gold-covered silicon and germanium were also acquired and compared to the spectrum of sputtered gold. The Au $4f_{7/2}$ peaks were centered at 84 eV, and the Au $4f_{5/2}$ at 87.7 eV. Shifts of the gold core levels were not observed in our experimental conditions for either silicon or germanium samples.

Angle resolved analyses of the XPS core levels were carried out. At the glancing detection angle of 80°, the Si 2p peak remained centered at about 99 eV and the intensity of the silicon dioxide peak increased with gold coverage, becoming comparable to the intensity of the silicon core peak. The deconvolution of the experimental germanium core peak shows the shift of the elemental Ge 3d by about 0.2−0.3 eV and the growth of the germanium oxide peak at about 31.2 eV with gold coverage, consistent with the deconvoluted normal incidence data.

The core peak analyses of the displacement gold/semiconductor systems provided only limited information about the interaction between the metal and the semiconductor. The appearance, with gold coverage, of the peak at 103 eV for silicon and of the very small deconvoluted peak at 31.2 eV for

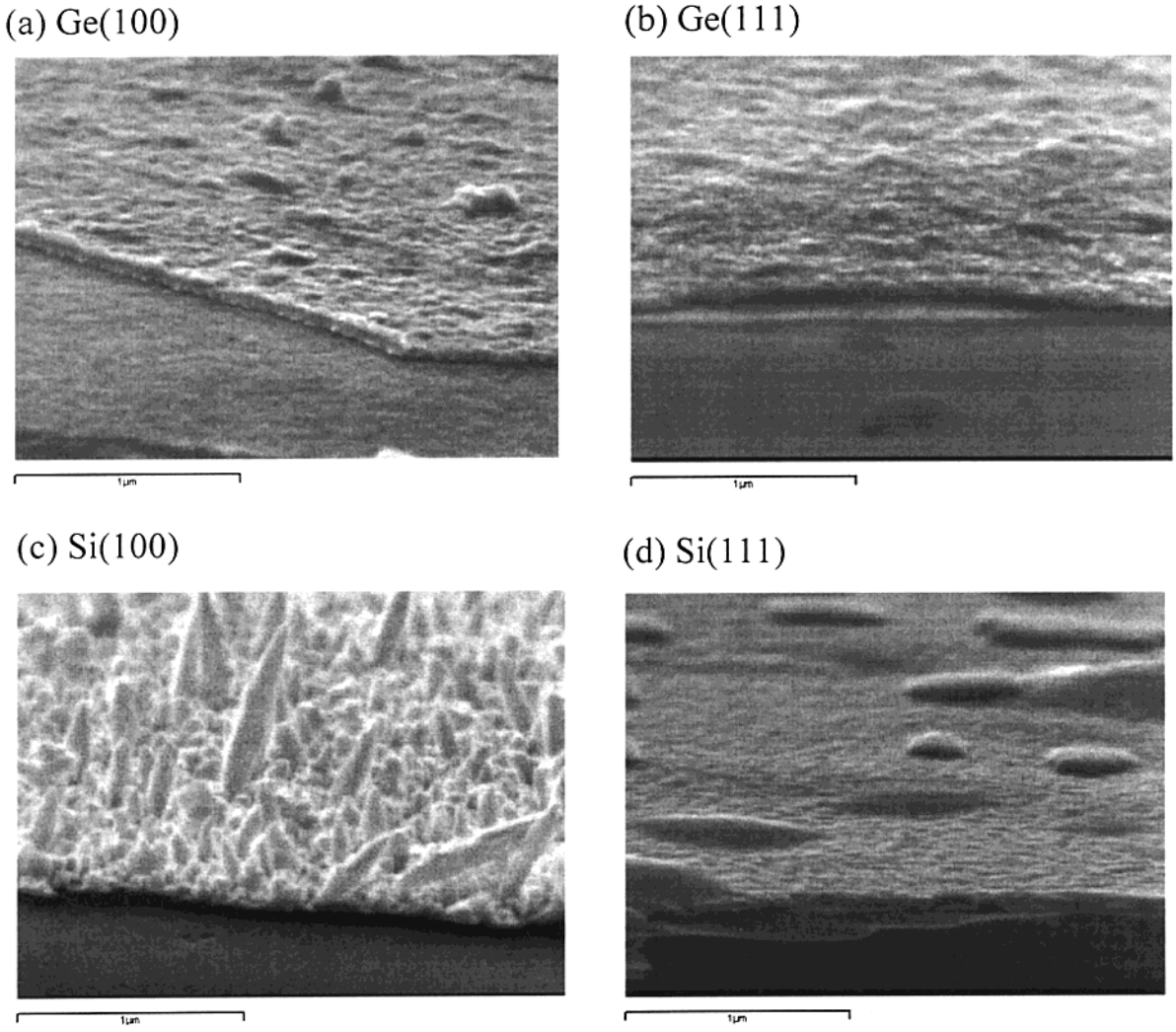

Figure 3. Scanning electron micrographs of samples plated for 30 min in 1 mM Au bath.

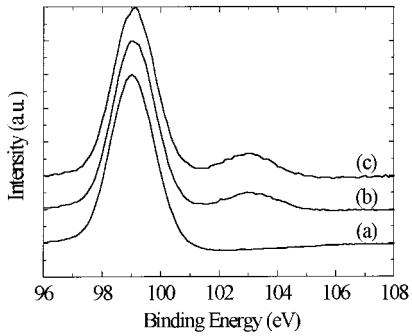

Figure 4. X-ray photoemission spectra of Si 2p core level peak for clean Si (a) and after immersion plating for 5 s (b) and 60 s (c).

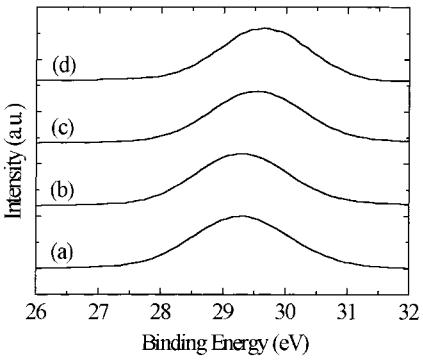

Figure 5. X-ray photoemission spectra of Ge 3d core level peak for clean Ge (a) and after immersion plating for 5 s (b), 60 s (c), and 600 s (d).

germanium suggests that the presence of the metal enhances the formation of oxides for both silicon and germanium. The reason for the enhanced oxidation can be traced to the galvanic coupling between Au and semiconductor substrate.[18] Furthermore, in the case of germanium, the 0.2−0.3 eV shift of the elemental Ge peak at nonzero Au coverage is indicative of a chemical interaction and is in agreement with previous synchrotron studies of the Au/Ge interface formed in a vacuum.[19] The analysis of the valence band (VB) spectra, described below, bears out more striking signature of such interaction and points to the formation of the stoichiometric compound Au_3Ge.

Valence band spectra in the range from −2 eV to 14 eV were collected for silicon and germanium with increasing gold coverage, as well as for a thick sputtered gold film as a reference. Decomposition of the valence band spectra using Gaussian peaks was carried out. The fwhm of the peaks was derived from the band decomposition of the reference sputtered gold and fixed at 2.7 eV; two peaks at 3.2 and 6.1 eV for the pure Au valence band were identified, as shown in Figure 6. They correspond to the Au $5d_{5/2}$ and $5d_{3/2}$ levels, respectively. The observed splitting of 2.9 eV is in very good agreement with the experimental value of 2.75 eV for pure Au.[20]

Figure 7 shows the comparison of the valence bands of clean silicon (a) and after immersion in the plating solution for 5 s (b) and 60 s (c). The deconvolution of the valence bands for gold-covered silicon, where Au 5d band peaks were centered at the reference binding energies of pure Au, is reported. Valence bands were composed of two main Au 5d peaks, with no other peaks attributable to gold. The residual curve, i.e., the difference between the experimental data and the peaks fitted based on the valence band structure of the reference gold, reproduced quite reasonably the substrate contribution to the valence band spectrum. Increasing plating time (and thus gold coverage) increases the Au 5d contribution as well as the density of states

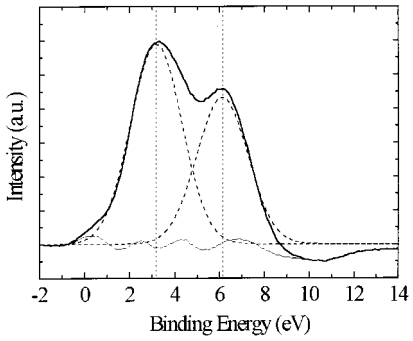

Figure 6. X-ray photoemission spectra of the valence band region of a 1.5 μm-thick sputtered gold sample. The peaks at 3.2 and 6.1 eV binding energy correspond to the Au $5d_{5/2}$ and Au $5d_{3/2}$ levels, respectively. Thick solid line: data. Dashed line: fitted peaks. Thin solid line: residual.

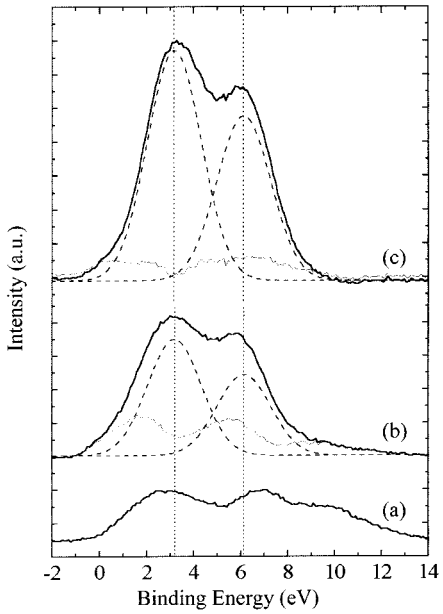

Figure 7. X-ray photoemission spectra of the valence band region of clean (a) and Au plated [5 s (b) and 60 s (c)] Si. Thick solid line: data. Dashed line: fitted peaks constrained to the Au 5d binding energy values. Thin solid line: residual.

at binding energy BE = 0, as expected. To summarize: the experimental spectra of gold-covered silicon can be decomposed into the contribution of pure gold and clean silicon. Shifts of the peaks related to overlapping bands were not observed.

In Figure 8, the experimental valence band photospectra for germanium as clean (a) and after immersion in the gold plating solution for 5 s (b), 60 s (c), and 600 s (d) are reported. Spectra of germanium coated with gold showed a shift of the main peak toward higher binding energies and an increased density of states at binding energy BE = 0. The line shape decomposition of the band spectra for gold-covered germanium comprised the two Au 5d peaks fixed at 3.2 and 6.1 eV binding energies. The theoretical Gaussian peak at 3.2 eV was characterized by a small intensity for shorter plating times. However, the deconvolution revealed a second intense peak at 3.7 eV after 5 s deposition. This peak is shifted by 0.5 eV toward higher binding energies with respect to the clean Au VB peak and it is attributed to the interaction of the metal with the germanium substrate. Spectra acquired at the glancing angle of 80° confirmed the 0.5 eV shift observed at normal incidence. At high gold coverage, i.e., after deposition for 600 s, the intensity of this peak becomes smaller compared to the growing Au 5d peak at 3.2 eV, confirming

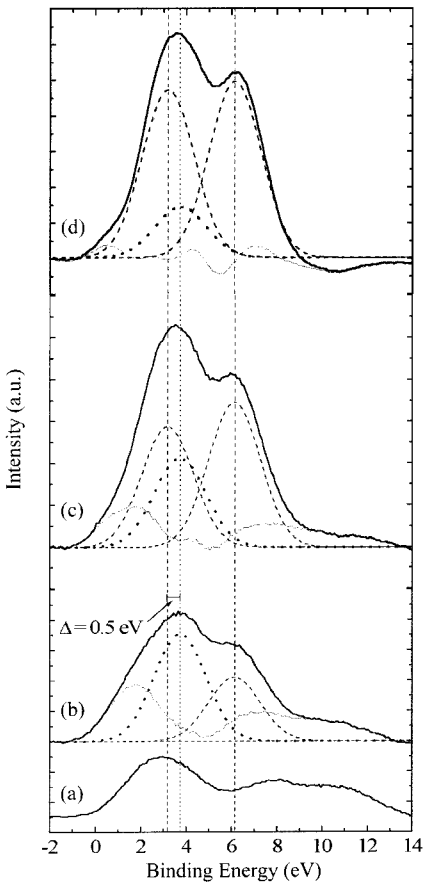

Figure 8. X-ray photoemission spectra of the valence band region of clean (a) and Au plated [5 s (b), 60 s (c), and 600 s (d)] Ge. Thick solid line: data. Dashed line: fitted peaks constrained to the Au 5d binding energy values. Dashed line: fitted peak at 3.7 eV BE. Thin solid line: residual. The new peak at 3.7 eV binding energy is attributed to the interaction of the Au $5d_{5/2}$ electrons with Ge 4(sp) orbitals.

that the strong Au−Ge interaction remains confined to a thin interfacial region.

IV. Discussion and Conclusion

Gold films deposited on Si and Ge substrates by the galvanic displacement method display remarkably different interfacial behavior. Specifically, the Au−Si interface is mechanically weak and no chemical interaction between the two elements is detected by photoelectron spectroscopy of either core or valence levels. In contrast, the Au−Ge system displays excellent interfacial adhesion, presumably originating in the strong chemical interaction between the two species. Indeed, photospectra show shifts of the Ge core levels as well as a new structure in the valence band.

In the absence of previous studies of interfacial formation during the galvanic displacement process, one can gain some insight in the process by turning to theoretical and experimental work on the electronic structure of Au−semiconductor interfaces formed in a vacuum.[19,21−30]

The occurrence of solid-state reactions at the interface between gold films and silicon or germanium has been evaluated at different temperatures, revealing significant differences between the two semiconductors. Despite the fact that the binary alloy phase diagrams[31] for Au/Si and Au/Ge appear similar and both are characterized by eutectic phases, several authors reported the formation of gold silicide and germanide with different structure. For the Au/Si system, an intermixing reaction has been reported to occur and produce a Si-metal alloyed interface with amorphous structure.[21−23] Gheber et al.[24] investigated the interface formation between hydrogen-terminated Si(111) and evaporated gold. They observed that the first monolayers of gold deposited at room temperature onto H-terminated Si(111) covered the silicon surface uniformly and formed Au−Si chemical bonds (in significant contrast with our observation following galvanic displacement). Gold silicide formation was observed by Sundaravel et al.[25] after deposition of gold thin film under high vacuum conditions on a chemically prepared bromine passivated Si(111) substrate *and* annealing around eutectic temperature. Chemical shifts in the XPS peaks of Si 2p and Au 4f were detected, and an average composition of Au_4Si was attributed to the silicide compound. Perfetti et al.[19,26,27] investigated the formation of the Ge/Au interface (in a vacuum at room temperature) and compared it to the Si/Au interface. They found that, unlike gold on silicon, gold on germanium formed a phase of well-defined stoichiometry at the interface. Comparison with theoretical calculations suggested the formation of a stoichiometric Au_3Ge compound. The valence band region showed new spectral structure that depends on gold coverage: as a consequence of the bonding between Au d-states and Ge p-orbitals, two additional d-structures appeared in the photospectra between −2 and −3 eV and between −8.3 and −10 eV below the Fermi level. The bulk Au d-band is located between −3 and −7 eV from the Fermi level. Le Lay et al.[28,29] confirmed that the gold overlayer deposited at room temperature on germanium strongly modified the surface electronic properties. Diffraction experiments revealed the formation of a well-defined structure, which is quite different from the amorphous alloyed phase at the Si/Au interface. Subsequent scanning tunneling and photoelectron spectroscopy measurements[30] at surface coverage of 1/3 of a monolayer were consistent with the formation of Au_3Ge molecules.

These results shed light on our studies of the Au/Si and Au/Ge interfaces obtained by immersion plating of the semiconductors in fluoride-containing solutions of a gold salt. Our XPS results show the formation of a chemical bond at the Au/Ge interface, which can most likely be attributed to a stoichiometric compound. In contrast, no bonding can be detected in the Au/Si system. We propose the formation of an interfacial stoichiometric compound as the cause of the excellent adhesion observed in the former system. Additional evidence for this mechanism of interfacial adhesion will be sought in future studies involving other transition metals with known propensity for stoichiometric compound formation on Si, such as Pd and Pt.

Acknowledgment. This work was supported in part by Sandia National Laboratories and by the Arnold and Mabel Beckman Foundation.

References and Notes

(1) Chyan, O. M. R.; Chen, J. J.; Chien, H. Y.; Sees, J.; Hall, L. *J. Electrochem. Soc.* **1996**, *143*(1), 92−96.

(2) Jeon, J. S.; Raghavan, S.; Parks, H. G.; Lowell, J. K.; Ali, I. *J. Electrochem. Soc.* **1996**, *143*(9), 2870−2875.

(3) Lee, M. K.; Wang, H. D.; Wang, J. J. *Solid-State Electron.* **1997**, *41*(5), 695−702.

(4) dos Santos F, S. G.; Martins, L. F. O.; D'Ajello, P. C. T.; Pasa, A. A.; Hasenack, C. M. *Microelectron. Eng.* **1997**, *33*, 59−64.

(5) dos Santos F, S. G.; Pasa, A. A.; Hasenack, C. M. *Microelectron. Eng.* **1997**, *33*, 149−155.

(6) Lee, M. K.; Wang, J. J.; Wang, H. D.; *J. Electrochem. Soc.* **1997**, *144*(5) 1777−1780.

(7) Gorostiza, P.; Diaz, R.; Sanz, F.; Morante, J. R. *J. Electrochem. Soc.* **1997**, *144*(12), 4119−4122.

(8) Li, G.; Kneer, E. A.; Vermiere, B.; Parks, H. G.; Raghavan, S.; Jeon, J. S. *J. Electrochem. Soc.* **1998**, *145*(1), 241−246.

(9) Cheng, X.; Li, G.; Kneer, E. A.; Vermiere, B.; Parks, H. G.; Raghavan, S.; Jeon, J. S. *J. Electrochem. Soc.* **1998**, *145*(1), 352−357.
(10) Gorostiza, P.; Anbu Kulandainathan, M.; Diaz, R.; Sanz, F.; Allongue, P.; Morante, J. R. *J. Electrochem. Soc.* **2000**, *147*(3), 1026−1030.
(11) Srinivasan, R.; Suni, I. I. *Surf. Sci.* **1998**, *408*, L698-L702.
(12) Srinivasan, R.; Suni, I. I. *J. Electrochem. Soc.* **1999**, *146*(2), 570−573.
(13) Rossiter, C.; Suni, I. I. *Surf. Sci.* **1999**, *430*, L553-L557.
(14) Balashova, N. A.; Eletskii, V. V.; Medyntsev, V. V. *Elektrokhimiya* **1965**, *1*, *3*, 274−278.
(15) Krikshtopaitis, I. B.; Kudzhmauskaite, Z. P. *Elektrokhimiya* **1971**, *7*, *10*, 1579−1581.
(16) Magagnin, L.; Maboudian, R.; Carraro, C. *Electrochem. Solid-State Lett.* **2001**, *1*, C5−C7.
(17) Li, J.; Blewer, R.; Mayer, J. W. *Mater. Res. Soc. Bull.* **1993**, *18*, 18−18.
(18) Kim, J. S.; Morita, H.; Joo, J. D.; Ohmi, T. *J. Electrochem. Soc.* **1997**, *144*, 3275−3283.
(19) Perfetti, P.; Katnani, A. D.; Zhao, T.-X.; Margaritondo, G.; Bisi, O.; Calandra, C. *J. Vac. Sci. Technol.* **1982**, *21*(2), 628−631.
(20) Kuhn, M.; Sham, T. K. *Phys. Rev. B* **1994**, *49*, 1647−1658.
(21) Hiraki, A. *Surf. Sci. Rep.* **1984**, *3*, 357−412.
(22) Calandra, C.; Bisi, O.; Ottaviani, G. *Surf. Sci. Rep.* **1985**, *4*, 271−364.
(23) Ceelen, W. C. A. N.; Moest, B.; de Ridder, M.; van Ijzendoorn, L. J.; Denier van der Gon, A. W.; Brongersma, H. H. *Appl. Surf. Sci.* **1998**, *134*, 87−94.
(24) Gheber, L. A.; Hershfinkel, M.; Gorodetsky, G.; Volterra, V. *Thin Solid Films* **1998**, *320*, 228−235.
(25) Sundaravel, B.; Sekar, K.; Kuri, G.; Satyam, P. V.; Dev, B. N.; Bera, S.; Narasimhan, S. V.; Chakraborty, P.; Caccavale, F. *Applied Surface Science* **1999**, *137*, 103−112.
(26) Perfetti, P.; Katnani, A. D.; Daniels, R. R.; Zhao, T.-X.; Margaritondo, G. *Solid State Commun.* **1982**, *41*(3), 213−215.
(27) Quaresima, C.; Sette, F.; Patella, F.; Savoia, A.; Perfetti, P. *Solid State Commun.* **1982**, *44*(8), 1165−1169.
(28) Le Lay, G.; Manneville, M.; Metois, J. J. *Surf. Sci.* **1982**, *123*, 117−128.
(29) Le Lay, G. *Surface Science* **1983**, 132, 169−204.
(30) Gothelid, M.; Hammar, M.; Bjorkqvist, M.; Karlsson, U. O.; Flodstrom, S. A.; Wigren, C.; LeLay, G. *Phys. Rev. B* **1994**, *50*, 4470−4475.
(31) *Binary Alloy Phase Diagrams*; American Society for Metals: Metals Park, Ohio, 1987; pp 263−264, 312−313.